Journal Pre-proof

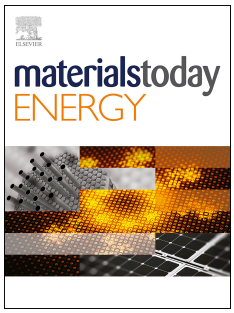

Optimization of H_2O_2 production in small-scale off-grid buffer layer flow cell equipped with Cobalt@N-Doped Graphitic Carbon Core–Shell Nanohybrid electrocatalyst

Jonathan Filippi, Hamish A. Miller, Lucia Nasi, Maria V. Pagliaro, Andrea Marchionni, Michele Melchionna, Paolo Fornasiero, Francesco Vizza

PII: S2468-6069(22)00150-2

DOI: https://doi.org/10.1016/j.mtener.2022.101092

Reference: MTENER 101092

To appear in: *Materials Today Energy*

Received Date: 26 April 2022

Revised Date: 4 July 2022

Accepted Date: 5 July 2022

Please cite this article as: J. Filippi, H.A. Miller, L. Nasi, M.V. Pagliaro, A. Marchionni, M. Melchionna, P. Fornasiero, F. Vizza, Optimization of H_2O_2 production in small-scale off-grid buffer layer flow cell equipped with Cobalt@N-Doped Graphitic Carbon Core–Shell Nanohybrid electrocatalyst, *Materials Today Energy*, https://doi.org/10.1016/j.mtener.2022.101092.

Credit Author statement

Jonathan Filippi **Conceptualization; Data curation; Formal analysis; Investigation; Methodology; Roles/Writing – original draft; Writing – review & editing**

Hamish A. Miller **Methodology; Validation; Roles/Writing – original draft; Writing – review & editing**

Lucia Nasi **Investigation**

Maria V. Pagliaro **Conceptualization; Investigation; Methodology**

Andrea Marchionni **Software; Visualization; Writing – review & editing**

Michele Melchionna **Conceptualization; Data curation; Investigation; Roles/Writing – original draft; Writing – review & editing**

Paolo Fornasiero **Conceptualization; Formal analysis; Resources; Software; Supervision; Validation; Roles/Writing – original draft; Writing – review & editing**

Francesco Vizza **Conceptualization; Data curation; Funding acquisition; Project administration; Resources; Supervision; Validation; Roles/Writing – original draft; Writing – review & editing**

Optimization of H_2O_2 production in small-scale off-grid buffer layer flow cell equipped with Cobalt@N-Doped Graphitic Carbon Core–Shell Nanohybrid electrocatalyst

Jonathan Filippi,[a] Hamish A. Miller,[a] Lucia Nasi,[b] Maria V. Pagliaro,[a] Andrea Marchionni,[a] Michele Melchionna,[c] Paolo Fornasiero,*[c,d], Francesco Vizza*[a]

a. ICCOM-CNR, via Madonna del Piano 10, 50019 Sesto Fiorentino (FI), Italy. E-mail: francesco.vizza@iccom.cnr.it

b. CNR-IMEM Institute, Parco area delle Scienze 37/A, 43124 Parma, Italy

c. Department of Chemical and Pharmaceutical Sciences, Center for Energy, Environment and Transport Giacomo Ciamician, University of Trieste and Consortium INSTM, Via L. Giorgieri 1, 34127 Trieste, Italy. E-mail: pfornasiero@units.it

d. ICCOM-CNR, University of Trieste, Via L. Giorgieri 1, 34127 Trieste, Italy

Abstract:

Electrochemical oxygen reduction (ORR) to hydrogen peroxide (H_2O_2) is emerging as a sustainable approach for the production of "green" H_2O_2 requiring only oxygen and electricity compared to the energy intensive anthraquinone process. High $2e^-$ selectivity is required in order to boost faradaic and energy efficiency (FE) of the process. Upon correct tuning of their properties, nitrogen-doped carbon materials are excellent candidates as electrocatalyst for H_2O_2 electrosynthesis due to their chemical and electrochemical resistance and $2e^-$ selectivity. Furthermore, careful cell design and parameter optimization are mandatory for an industrial scale up of the process. In this study, a Cobalt@N-doped graphitic carbon core–shell nanohybrid (CS(Co)-N-GC) electrocatalyst was studied in a buffer layer complete cell equipped with a proton exchange membrane in order to determine the effect of flow rate and potential on process selectivity and energy efficiency. After optimization, the cell was able to produce 0.5 wt% H_2O_2 with an average FE higher than 40%, an energy consumption lower than 8 kWh kg_{H2O2}^{-1} and a production rate of 1.2 g h^{-1} g_{cat} @ 0.3V vs RHE with the possibility to produce up to 1 wt% H_2O_2.

Introduction:

Hydrogen peroxide can be considered an excellent "green" oxidant due to the absence of byproducts (except water) upon use, relatively high redox potential, and relative safety and low toxicity. Its uses range from organic compound oxidation, (paper pulp) bleaching, detergent, chemical synthesis, textile industry, waste water treatment and medical uses (disinfection, sanitization, cleansing).[1] Currently, nearly all hydrogen peroxide worldwide (6 million metric tons) is produced by the energy intensive Anthraquinone process, that involves several steps of

reaction and separation followed by distillation.[1,2] To be economically sustainable the anthraquinone process requires very large scales and centralized production that also pose several safety issues due the high concentration needed for efficient transportation (above 60%) requiring distillation prior to shipping. Therefore, this also has a very strong impact on the total energy consumption of the H_2O_2 production process, ranging between 12 and 17 kWh kg_{H2O2}^{-1}.[2] In addition, many final uses require relatively low concentrations: for example, medical uses where the concentration is often less than 3% for example, [3-7] H_2O_2 can be used effectively for the disinfection of surfaces and ambient from Sars-Cov-2 virus with a concentration of 0.5 wt%. Decentralizing the production of H_2O_2 can promote effectively the access to cheap disinfectants in remote areas aiding the fight against the pandemic. One interesting decentralized H_2O_2 production approach is the electrosynthesis via oxygen reduction reaction (*ORR*) requiring, in principle, only oxygen (air), water and electricity.[8-10] In order to produce H_2O_2, the reaction should proceed through the 2 electron pathway, as any spurious 4 electron process reduces severely the current efficiency (and hence energy efficiency) of the entire process.[8,11-12] Hydrogen peroxide stability is also an issue. Many metal nanoparticle based electrocatalysts demonstrate interesting performance and efficiency both in half cells and in full cells, [8,13-17] but material supply limitations and cost and metal leaching phenomena can significantly limit the applicability, efficiency and durability of this technology. Materials development for ORR needs to take into careful consideration the differences in synthetic conditions, as small variations can lead to remarkably different catalytic behaviors. Encapsulated transition metals into carbon nanostructures have been reported with various metals such as Fe and Co and various nanocarbon morphology, exhibiting profound activity and selectivity differences in ORR.[18-21], In addition, the use of heteroatom-doped carbon-based metal free electrocatalysts[17-38] can overcome many of the limitations posed by metal nanoparticle electrocatalysts, such as leaching and passivation. Another possible approach is to embed the metal in a nitrogen-doped graphitic core-shell structure, in which the electronic levels of the carbon and the nitrogen are affected by the presence of the core metal,[18] which can be favorably tuned to boost two electron ORR selectivity.[39,44]. In addition, some nitrogen functionalities such as graphitic, pyrrolic, pyridinic are known to promote the 2e- oxygen reduction reaction mechanism.[38,43] In a previous work, a Cobalt@N-doped graphitic carbon core–shell nanohybrid electrocatalyst (CS(Co)-N-GC) has been shown to demonstrate high H_2O_2 selectivity (up to 98% faradaic efficiency, FE) in half cells and at low overpotential.[44] Departing from ideal model studies, performed with techniques such as RRDE (rotating ring-disk electrode), it is important to consider that practical complete cell performance is also affected by O_2 and H_2O_2 transport phenomena (in particular H_2O_2 residence times) and reaction media (interfering ions and pH) affecting H_2O_2 stability.[45,46] The use of a GDL can effectively promote O_2 transport at the cathode without O_2 electrolyte solubility limitations.[39-42,46-48] Another important consideration is that forced convention (RRDE) experiments tend to overestimate the H_2O_2 selectivity compared to practical systems:[12,45] H_2O_2 concentration buildup, although highly desirable, can severely affect the reaction selectivity since it translates in an increase of H_2O_2 concentration at the electrode interface, that can result in its further reduction to H_2O or non-electrochemical disproportionation to O_2 and water. Chuan at al. [49] described a GDL-based complete cell able to withstand up to 20% H_2O_2 by using a porous

layer separator with a membrane on each side (acidic at the anode, alkaline at the cathode) designed to recombine HO_2^- produced at the cathode with H^+ (from H_2 oxidation reaction) produced at the anode without contact of the resulting neutral H_2O_2 with the electrodes. This very promising approach still depends on the availability of gaseous H_2 for the anode, limiting its applicability in remote areas. Tuning the residence times and potentials can control effectively parasitic phenomena limiting the FE and increasing the energy requirements of the process.[12] Summarizing, most studies are conducted in half cells to have a first scrutiny of the performance, with limited but relevant investigations on full devices.[49] The present study provides a contribution on the cell engineering in order to minimize the performance losses with respect to the bench tests, and it is a key step for the implementation of real devices. Therefore, we describe the optimization of a two compartment gas diffusion layer flow cell equipped with a **CS(Co)-N-GC** electrocatalyst. Results indicate the possibility to produce build up a concentration of in solution up to 0.5 wt% H_2O_2 with an average faradaic efficiency higher than 40% and up to 1 wt% with an average faradaic efficiency higher than 20%, with an energy demand lower than that of the anthraquinone process when limiting the concentration to 0.8 wt% H_2O_2.

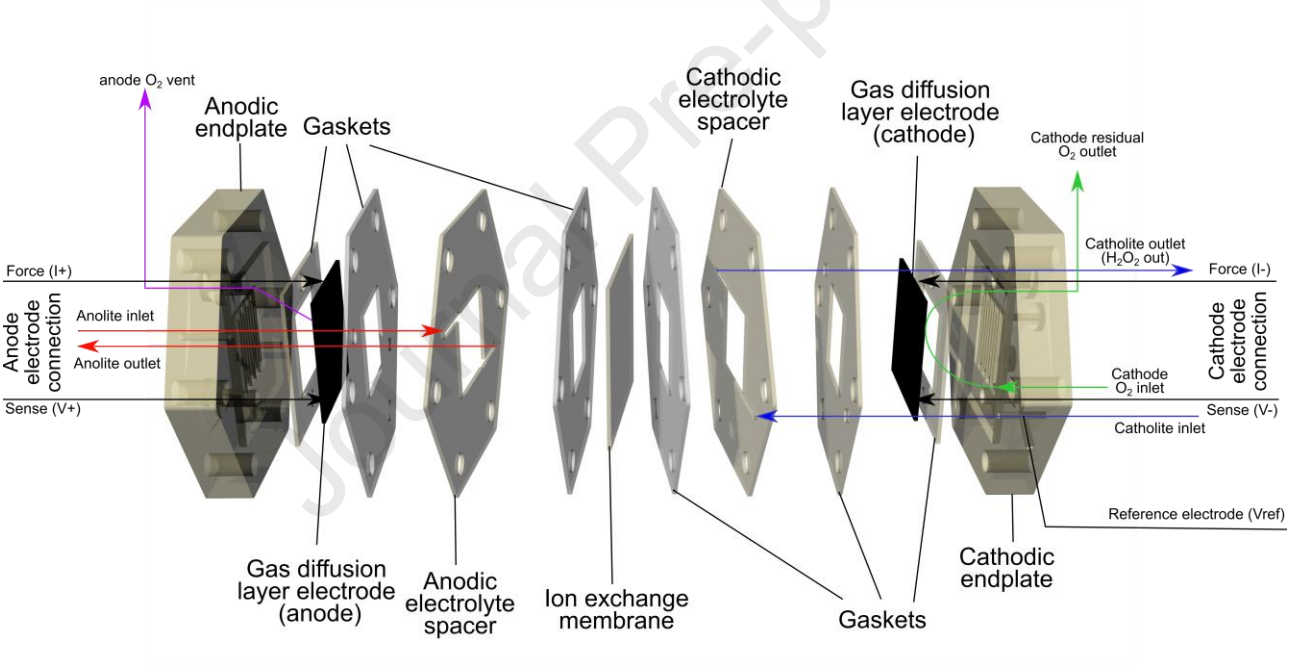

Figure 1: double buffer layer, gas diffusion H_2O_2 electrosynthesis cell structure

2 Methods:

2.1 Synthesis of the electrocatalysts

2.1.1 Synthesis of Cobalt@N-Doped graphitic carbon core–shell nanohybrid electrocatalyst electrocatalyst (CS(Co)-N-GC).

The **CS(Co)-N-GC** nanomaterial was synthesized as described in [44]. The synthesis of the electrocatalyst was performed by thermal decomposition. A 1:1 solution of $Co(ac)_2{\cdot}4H_2O$ (Merck ACS reagent, ≥98.0%) and a nitrogen-bearing organic precursor (imidazole, Merck ACS reagent

≥99.0%) was prepared and agitated overnight. The solvent was then removed, and the as-obtained solid was transferred into an open alumina ceramic vessel and treated in a tubular furnace under Ar flow in order to remove oxygen. After 1.5 h at 40°C under Ar atmosphere, the temperature was raised to 900°C with a ramp of 5°C min^{-1} and hold for 2 h before cooling of the vessel to room temperature, the obtained pyrolyzed material was then ground by using an agate mortar to obtain a fine powder. It was then dispersed in 0.5M $HClO_4$ (Merck) and subsequently stirred at 80 °C for 4 h in order to remove eventual exposed metal impurities. The acid-treated sample was filtered and washed with water. The procedure was repeated twice, and then the obtained black powder was dried under vacuum and recovered.

2.1.2 Cathode preparation on carbon cloth

20mg of **CS(Co)-N-GC** were dispersed ultrasonically for 60 minutes in mixture of 1.5 g 2-propanol (Merck ACS reagent, ≥99.5%) and 0.5g of milliQ water, together with 65mg of a 5 wt% nafion oligomer solution in lower aliphatic alcohols (Merck). The uniform ink obtained was casted by subsequent deposition-drying cycles on a 37x37mm carbon cloth support (GPP050M from Cetech Co. ltd) previously cleaned ultrasonically and tape-masked to expose an area of 6.25 cm^2 (figure S1). **CS(Co)-N-GC** loading (1.6-1.9 mg cm^{-2}) was estimated by weight difference.

2.1.3 IrO_2 anode preparation on carbon cloth

20mg of powdered IrO_2 electrocatalyst mixed in a mortar with 25mg of Vulcan XC-72 carbon (Cabot) were dispersed ultrasonically for 60 minutes in mixture of 1.5 mg 2-propanol and 0.5 g of water, together with 96 mg of a 5 wt% nafion oligomer solution in lower aliphatic alcohols. The uniform ink obtained was casted by subsequent deposition-drying cycles on a 37x37mm carbon cloth support (GPP050M from Cetech Co. ltd) previously cleaned ultrasonically and tape-masked to expose an area of 6.25 cm^2 (see scheme S1) until the maximum possible loading on the surface was achieved. The IrO_2 loading (3 mg cm^{-2}) was estimated by weight difference.

2.2 Electrochemical reactor experiments

Electrochemical reactor experiments were conducted in a 3D-printed ASA (acrylonitrile styrene acrylate) gas diffusion flow reactor (figure 1, S2, S3) equipped with two flow buffer layers (cathode and anode) with a circulating 0.1N H_2SO_4 (Sigma Pure PA) solution in milliq water on both compartments. Both the two liquid circuits (anode and cathode) were circulated by a Gilson peristaltic pump equipped with Tygon™ tubes. The cell, vertically oriented has four compartments: starting from cathode side, i) a gas compartment where pure O_2 (Air-liquide 99.95% purity) was flowed continuously at atmospheric pressure; the gas diffusion electrode with the oxygen reduction reaction electrocatalist (CS(Co)-N-GC) was housed at the interface between the gas compartment and the cathode buffer layer; liquid and gas tightness was ensured by two hexagonal rubber gaskets with the additional purpose of masking the active area (25 x 25 mm, 6.25 cm^2 exposed surface; ii) and iii) cathodic and anodic buffer layers flowing through the channels left by the spacers between the electrodes and the Nafion 117 membrane; and iv) the anode gas compartment where water oxidation reaction (WOR) takes place. The anode buffer layer and the anode gas compartment were separated by the carbon cloth GDL covered with IrO_2

WOR electrocatalyst. The cathode feeding channel housed also the reference electrode ($Ag|AgCl|KCl_{sat}$) in close proximity to the cathode electrocatalyst to minimize the uncompensated resistance. The buffer layers were filled with circulating 0.05M H_2SO_4 (Merck Pure PA) and O_2 was fed continuously to the cathode gas compartment to ensure proper mass transport. Two different experiment types were performed: i) single pass experiments where the electrolyte, enriched with synthesized H_2O_2 by oxygen reduction reaction, was not recycled and was directly collected into the final tank and ii) recirculation experiments, where the electrolyte was continuously recirculated into the cathodic chamber during the experiment.

The flow rate were adjusted from 0.28 and 13.7 mL min^{-1} for buffer layers and the cathode potential was set in a range from 0.5 V to 0.1 V vs RHE. The total cell potential was measured by an external voltmeter in order to calculate the energy consumption of H_2O_2 production. The current collectors were made of stainless steel in a control-sense double connector configuration (figure S2) to minimize the contact IR_{drop}. The solution was not allowed to come in contact with the steel to avoid Fe ions contamination inside the cell that would decompose the H_2O_2, lowering the efficiency. The collected H_2O_2 was sampled accordingly with the optimal concentration range of the analytical method chosen for the determination. H_2O_2 for tolerance experiments was purchased from Merck (35%, no stabilizers) and titrated prior to the experiment directly sampling from the cell before applying potential.

Air breathing proof-of-concept experiments were performed with the gas diffusion layers directly exposed to the room atmosphere by using open chamber and plates both on cathode and anode side.

The temperature was held constant at 25°C by circulating the electrolyte into a 50cm silicone coiled tube immersed into a thermostatic bath.

2.3 Product analysis

The collected sample solutions H_2O_2 concentrations and quantity were determined by permanganometric titration using a 2-2.5 mM potassium permanganate solution as titrant and indicator freshly prepared and standardized prior to each experiment using high purity sodium oxalate (dried at 80°C for 24 hours prior the preparation of the standard solution) as mother substance. The more concentrated H_2O_2 solutions were sampled by using an 50-1000ul Eppendorf automatic pipette and scaled accordingly. The faradaic efficiency was determined by comparing charge passed with the charge corresponding to the moles of H_2O_2 detected by using Equation 1. The anode compartment was analyzed in order to detect any H_2O_2 formation or membrane crossover that resulted in quantities lower or close to the detection limit of the technique and negligible compared to the total charge passed (less than 1% of the cathodic H_2O_2 detected)

$$FE = 5F\frac{V_{liq}M_{MnO_4^-}V_{eq}}{V_{smpl}Q_{tot}}$$

Equation 1: faradaic efficiency (FE); M_{MnO4-} is the molarity of the titrant; V_{eq} is the endpoint volume, Q_{tot} is the total charge passed in the experiment; V_{liq} is the total liquid sample volume; V_{smpl} is the volume of the sample effectively titrated; F is Faraday's constant 96 485 A mol^{-1}.

2.3 Electrocatalyst durability analysis

In order to determine any morphological changes to the electrocatalyst over a long period of H_2O_2 electrosynthesis, after the long H_2O_2 production experiment, the cathode of the flow cell was recovered, washed with deionized water, dried under a current of N_2, and then the electrocatalyst powder was removed from the carbon cloth by mechanical scraping. The powder was then analyzed with Transmission Electron Microscopy (TEM) using a JEOL 2200FS microscope working at 200 kV, equipped with a High-Angle Annular Dark-Field (HAADF) detector, an in-column omega filter; the microanalysis was performed with an Energy-Dispersive X-ray (EDX) spectroscometer. The pristine electrocatalyst powder morphological and compositional was carried out using a Tescan GAIA 3 FIB/SEM microscope equipped with an Edax EDS Octane detector. Both Images and EDS compositional characterization were acquired using an impinging beam energy of 10 keV. Element distribution maps were acquired with a collection time of 600s.

3 Results and Discussion

The first set of experiments aimed at determining the optimum conditions for the electrocatalyst and the setup, in particular applied cathode potential and electrolyte flow rate. The first experiments at low flow rate were performed in "single pass" mode, without electrolyte recycling, in order to determine the effect of the fluid velocity; then the flow rate was further increased and the mode was switched to "recycle". The data obtained for the optimization of flow rate are shown in figure 2. The effect of the flow rate on energy efficiency is shown in the electronic SI (figure S4).

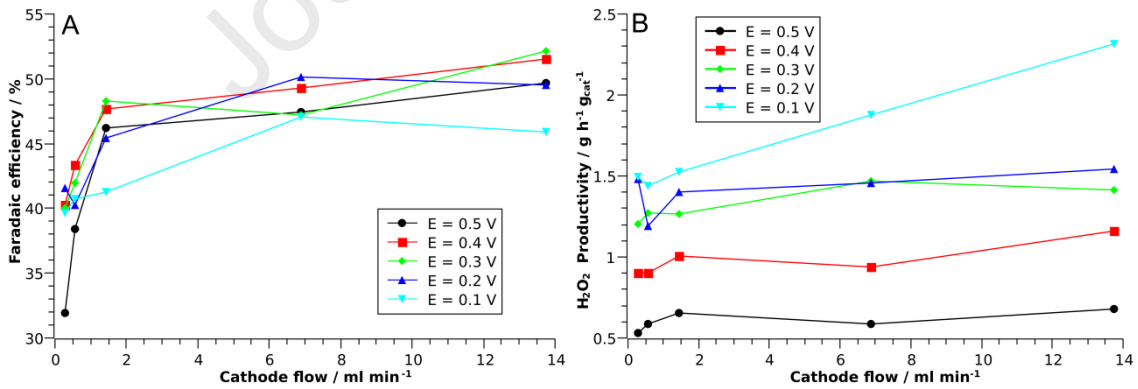

Figure 2: Cathode flow rate effect of faradaic efficiency (a) and on productivity (b) of the cell equipped with the CS(Co)-N-GC GDL cathode. The data points at 7 and 14 ml min^{-1} were performed in recirculation mode.

A higher flow rate was beneficial for the faradaic efficiency (FE_{H2O2}) as it reduces residence time and reduces the diffusion boundary layer thickness, speeding the mass transport and decreasing the cathode interface H_2O_2 concentration preventing its further reduction to H_2O. As stated

previously, forced convection experiments do not take into account H_2O_2 accumulation phenomena, due to fast mass transport and low bulk H_2O_2 concentration.

Regarding the effect of potential (figure 3), the more cathodic the potential was, the higher the current and the productivity; the FE increased till 0.3V vs RHE then started declining probably due to a promotion of 4 electron pathway rather than product accumulation, as the drop in selectivity seems more severe in stronger convection experiments ruling out a problem of H_2O_2 accumulation at the electrode interface. The peak FE was 52% @ 0.3V at a flow rate of 13.8 ml min^{-1}. The energy consumption per unit of H_2O_2 increased accordingly with the decline of faradaic efficiency and higher IR_{drop} in the cell and electrolyte remaining, though, remaining under 10 kWh kg_{H2O2}^{-1}.

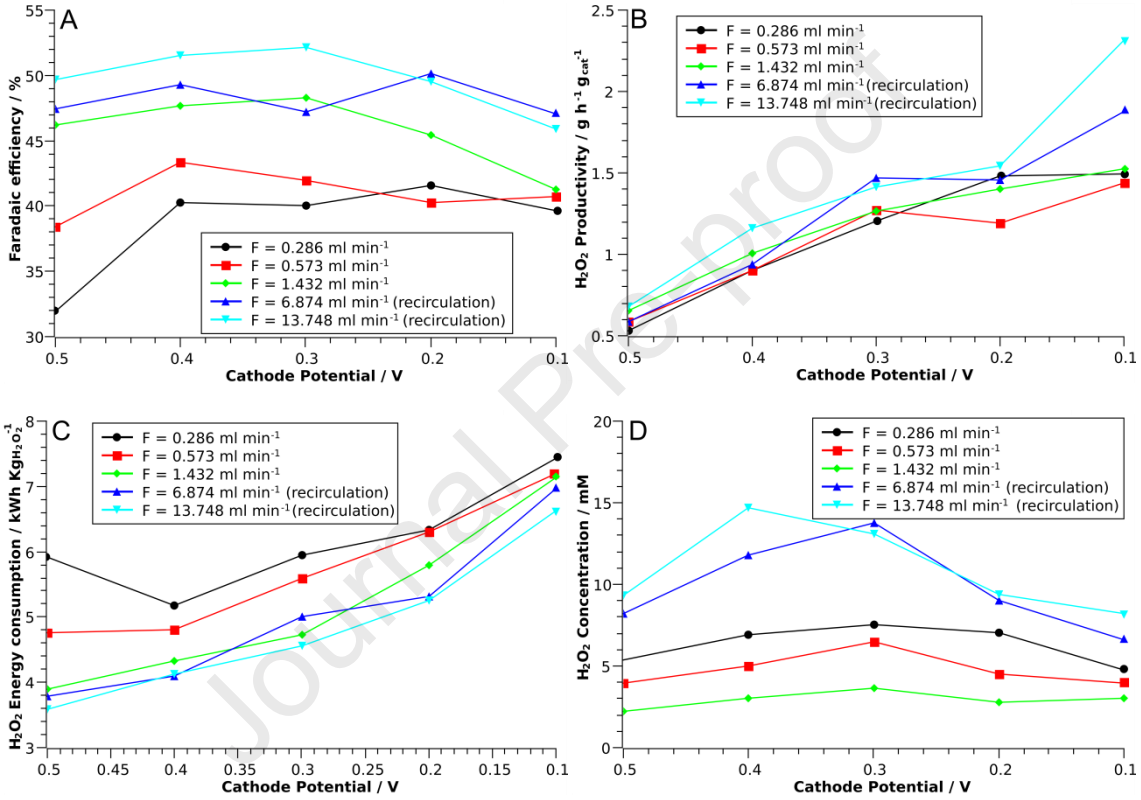

Figure 3: Cathode potential effect of FE (a), productivity (b), energy consumption (c) and H_2O_2 final concentration (d) of the cell equipped with the CS(Co)-N-GC GDL cathode. The points at 7 and 14 ml min^{-1} were performed in recirculation mode.

In order to survey the effect of hydrogen peroxide bulk concentration ($[H_2O_2]_{bulk}$) in the electrolyte on the faradaic efficiency, a series of experiments of H_2O_2 electrosynthesis in the presence of increasing starting hydrogen peroxide concentrations were performed (figure 4). Those experiments were designed to determine the impact of $[H_2O_2]$ on the selectivity excluding from the picture the electrocatalyst degradation that may occur in very long experiments. The conditions chosen for the experiments were 0.3V RHE and 13.8ml min^{-1} flow rate. The faradaic efficiency starts at 52% declining to 40% at 0.5 wt% H_2O_2, then rapidly declining to zero (production of H_2O_2 equals its degradation) at 0.9 wt%, getting negative (-4% FE) at 1.2 wt% indicating that H_2O_2 (which is added at the start of the experiment) is consumed by

decompositionrather than being solely produced at the cathode. The H_2O_2 partial current density decreased accordingly while the total current remained constant beyond 0.5 wt%. The maximum concentration attainable with this electrocatalyst in real conditions reported around 0.9 wt%. A long experiment (figure 5 and S5-S8), starting from zero $[H_2O_2]_{bulk}$, was also performed under the same conditions (0.3V vs RHE, 13.8 ml min^{-1}, 25°C). The FE_{H2O2} (figure S5) starts around 52% declining to 25% in 20 hours and to 0% in 55 hours. The H_2O_2 bulk concentration increases (figure S6) up to 1% where it reaches a plateau corresponding to 0% FE_{H2O2}.

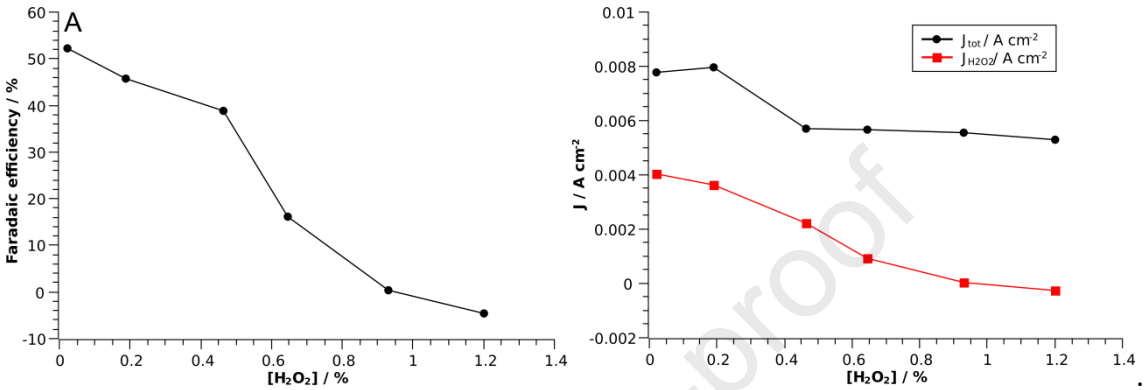

Figure 4: Faradaic efficiency (a) and on current densities (b) as a function of initial $[H_2O_2]$ for the complete cell equipped with the CS(Co)-N-GC GDL cathode at the optimal flow and potential condition.

Notably the FE_{H2O2} profile with respect to the concentration (figure 5a) declines rather linearly with the $[H_2O_2]_{bulk}$ reaching zero at 1 wt% . The same declining trend was observed with partial current and hence productivity starting from 3 g h^{-1} g_{cat}^{-1}. Interestingly, also the total current decreased suggesting that the H_2O_2 degradation could not be attributed to further reduction to H_2O but to a non-electrochemical disproportionation reaction at the interface. Replacing the solution with fresh electrolyte ($[H_2O_2]_{t=0}$ = 0) restored completely the FE_{H2O2} to 50% ruling out electrocatalyst degradation. For this reason, the maximum experiment time was limited to 50 hours due to the accumulation of H_2O_2 leading to the decrease of FE but a subsequent cycle produced nearly the same FE efficiency profile but a higher overall cell voltage due to the anode degradation. It is important to point out that very long operation times (total time > 2000 hours) request a careful design of membrane and anode to avoid their degradation, leading eventually to an increase in cell voltage and hence the decrease in total energy efficiency; in particular OER (oxygen evolution reaction) is very difficult in acidic media as corrosion of anode electrocatalyst is severe. Regarding the cathodic side, the-end-of-cycle *ex-situ* HAADF-STEM images, EDX elemental maps and High Resolution TEM (HRTEM) micrographs (figures 6, S12-S14) show the conservation of the core-shell structure of the electrocatalyst, with the absence of cobalt leaching phenomena outside the graphitic structure. In addition, surface SEM-EDAX mapping of pristine powder shows homogeneous distribution (figure S15-S17, table S1) of nitrogen and cobalt in the sample. Furthermore, analyzing the anode feed the total H_2O_2 detected accounted for less than 1% of the total charge passed, ruling out massive cross-over losses as the reason of such a decline in FE_{H2O2}. The energy consumption follows the same trend of the FE increasing massively beyond 0.6 wt% $[H_2O_2]_{bulk}$. Below this concentration the process outperforms anthraquinone process in terms of

energy demand [2], with the possibility or producing cheaper disinfectant-grade H_2O_2 on demand locally, requiring only water, air (oxygen) and electricity, that can be used for water purification, surface cleansing and disinfection uses. The reactor can be designed to limit the concentration below the 0.5 wt% threshold by continuously replacing (or diluting) the electrolyte circulating into the cell. The system can be easily scaled up for higher production rates. A 1 m^2 electrode assembly can produce continuously up to 4 liters h^{-1} of H_2O_2 0.5 wt% solution (20g H_2O_2) consuming less than 160W in the process (up to 32 liters daily in an 8 hour time using a 160W solar panel). Employing more H_2O_2-tolerant electrocatalysts and further improving mass transport (for example introducing vortex generators inside the electrolyte buffer layer) could increase the energy efficiency and the production rate even further.

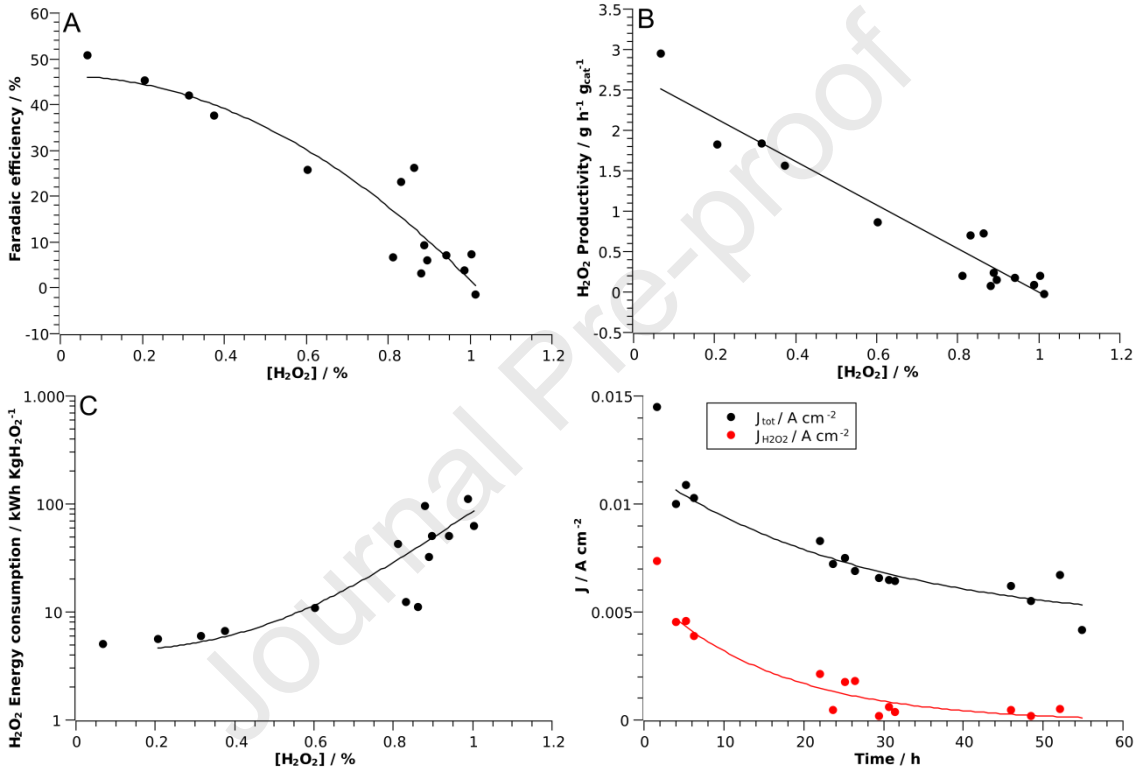

Figure 5: [H_2O_2] effect on faradaic efficiency (a), productivity (b) and energy consumption (c), partial and total current density time profile (d) during the 55 hours long H_2O_2 generation experiment performed with the cell equipped with the CS(Co)-N-GC GDL cathode.

We have reported a literature survey with some cases of cells (table 1) reporting, except one case with a peculiar cell configuration,[49] low maximum H_2O_2 concentrations attainable; this is due to the permanence of the H_2O_2 at the electrode leading to further reduction or disproportionation drastically reducing its FE.

A proof-of-concept experiment of an air-breathing system was also performed (figure S9-S11). The performance is lower than the setup using pure oxygen and the attainable concentration is roughly 25% of the experiment performed in pure oxygen, however this setup uses only water (1 mol per mol of H_2O_2), oxygen from air (1/2 mol per mol of H_2O_2) and electricity without the need to supply pure O_2 from a cylinder. Considering the same 10 kWh kg_{H2O2}^{-1} energy consumption

threshold to evaluate the performance, this setup can attain a concentration of 0.11 wt% H_2O_2 before the energy consumption becomes higher than that of the anthraquinone process.[2]

The mechanism of oxygen reduction to H_2O_2 has been extensively studied and follows the two step pathway:[37,38,43,45,46]

$O_2 + * + (H^+ + e^-) \rightarrow *OOH$

$*OOH + (H^+ + e^-) \rightarrow H_2O_2 + *$

Where $*$ represent an adsorption site.

We have previously shown how the selectivity towards H_2O_2 by N-doped carbon catalysts is strongly affected by the type and distribution of N moieties within the carbon as graphitic, pyrrolic, pyridinic are known to promote the 2e- oxygen reduction reaction mechanism.[36,38,43,50] Moreover, the porosity and textural properties of the materials play an important role due to the their effect on the mass transport, so that here the catalyst's structure is tailored to maximize efficiency in H_2O_2 production taking into account all these issues which we had been previously explored.[44]

Ref	Average Faradaic Efficiency	Maximum H_2O_2 concentration	Energy consumption kWh kg_{H2O2}^{-1}	Type of experiment	Average Current density
This paper	40%	0.5%	<8	BFL-O_2	8 mA cm^{-2}
	20%	0.11%	<10	BFL-Air	4 mA cm^{-2}
23	70-95%	0.2-0.75%	-	H-cell	4-12 mA cm^{-2}
39	>85	-	-	H-cell	0.15 mA cm^{-2}
44	>95%	-	-	H-cell	0.9 mA cm^{-2}
47	50-85%	-	4.6-19.4	BFL-Air	25-200 mA cm^{-2}
49	90%	20%	4.5 (including H_2)	H_2-anode fed, double membrane buffer layer fuel cell	300 mA cm^{-2}
51	50%	0.05%	9-11	BFL-O_2	50 mA cm^{-2}

Table 1: Literature overview of some H_2O_2 oxygen-reduction-based electrosynthesis experiments; BFL-O_2 = Buffer layer cell (pure O_2 fed); BFL-Air = Buffer layer cell (air breathing); H-cell = membrane-separated H-cell

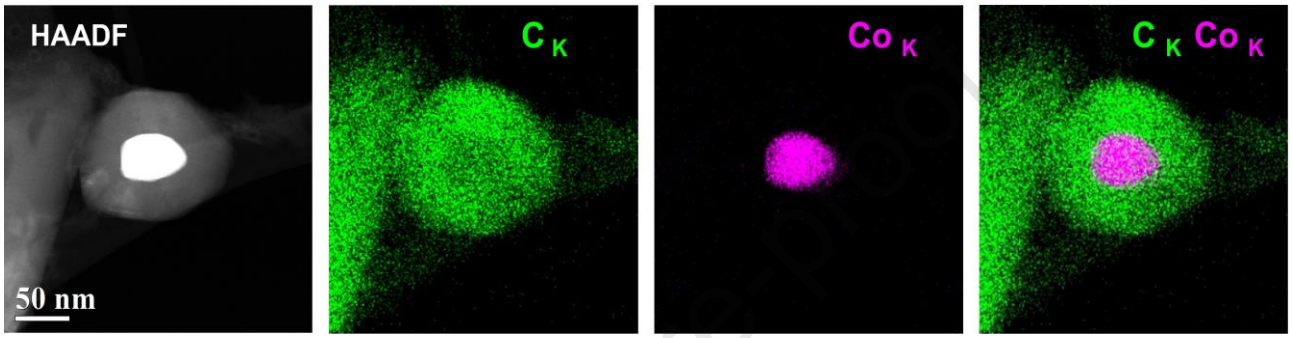

Figure 6: HAADF-STEM image and EDX elemental maps of the electrocatalyst after the long H_2O_2 electrosynthesis experiment, showing the conservation of the core-shell electrocatalyst structure.

4 Conclusions

In conclusion, a Cobalt@N-Doped graphitic carbon core–shell nanohybrid ORR electrocatalyst (CS(Co)-N-GC) operating in a complete gas-fed O_2 buffer layer electrochemical reactor was studied to determine the effect of flow rate and potential on process selectivity and energy efficiency. After optimization, the cell was able to produce continuously 0.5 wt% H_2O_2 with negligible electrocatalyst degradation attaining an average faradaic efficiency for H_2O_2 higher than 40%, consuming less than 8 kWh $kgH_2O_2^{-1}$ and demonstrating a production rate of 1.2 g h^{-1} g_{cat} @ 0.3V vs RHE corresponding to 4 liters of 0.5 wt% H_2O_2 each hour with an average energy consumption of 0.16 kWh and requiring only air, water and electricity. This will allow access to cheap and environmentally friendly disinfectants in remote areas, without the massive environmental footprint of centralized H_2O_2 production processes and their logistics. For future developments, the total energy balance must be also considered and careful design of the other cell parts (anode and membrane) are mandatory for a long term operation. In this work, the energy balance was limited to the electrical energy cost (excluding pumps and heating) as the experiment was designed as a table top lab scale proof of concept with laboratory apparatus (such as peristaltic pumps) with no long term cell operation assessment due to the scarce IrO_2 anode stability in the operation conditions. In, forthcoming studies, a full scale up of the system and an LCA analysis will allow to determine the total energy cost of H_2O_2 production through oxygen reduction reaction, in order to fathom for possible real device developments.

Acknowledgements

The Ente Cassa di Risparmio di Firenze (project EnergyLab) is kindly acknowledged for financial support. We acknowledge funding of a PRIN 2017 Project funded by the Italian Ministry MUR Italy (Grant No. 2017YH9MRK). We also acknowledge the Italian Ministry MISE for the FISR 2019 project AMPERE (FISR2019_01294).

References:

[1] J. M. Campos-Martin, G. Blanco-Brieva and Jose L. G. Fierro; *Angew. Chem. Int. Ed.* 2006, **45**, 6962 – 6984

[2] Goor, G., Glenneberg, J., Jacobi, S., Dadabhoy, J., & Candido, E. (2019). Hydrogen Peroxide. Ullmann's Encyclopedia of Industrial Chemistry, 1–40.

[3] G. Kampf, D. Todt, S. Pfaender, E. Steinmann; *Journal of Hospital Infection* 2020, **104**, 246-251.

[4] A. C. Ionescu, E. Brambilla, L. Manzoli, G. Orsini, V. Gentili, R. Rizzo; *Journal of Oral Microbiology* 2021, **13**, 1881361.

[5] D. Poppendieck, H. Hubbard, R. L. Corsi; Environ. Sci. Technol. Lett. 2021, **8**, 320−325.

[6] D. Mileto, A. Mancon, F. Staurenghi, A. Rizzo, S. Econdi, M. R. Gismondo, M. Guidotti; *ACS Chem. Health Saf.* https://doi.org/10.1021/acs.chas.0c00095.

[7] A. F. Capetti, F. Borgonovo, V. Morena, A. Lupo, M. V. Cossu, M. Passerini, G. Dedivitiis, G. Rizzardini; J. Med. Virol. 2021;93:1766–1769.

[8] Q. Zhao, J. An, X. Want, N. Li; *Int. J. Hydrogen Energy*, 2021, **46**, 3204-3219.

[9] S. Siahrostami, S. J. Villegas, A. H. B. Mostaghimi, S. Back, A. B. Farimani, H. Wang, K. A. Persson, J. Montoya; *ACS Catal.* 2020, **10**, 7495−7511.

[10] Z. Chen, S. Chen, S. Siahrostami, P. Chakthranont, C. Hahn, D. Nordlund, S. Dimosthenis, J. K. Nørskov, Z. Bao, T. F. Jaramillo; *React. Chem. Eng.* 2017, **2**, 239-245.

[11] Y. Wang, G. I. N. Waterhouse, L. Shang, T. Zhang; *Adv. Energy Mater.* 2021, **11**, 2003323.

[12] S. Anantharaj, S. Pitchaimuthu, S. Noda; *Advances in Colloid and Interface Science* 2021, **287**, 102331.

[13] K. Jiang, J. Zhao, *H. Wang; Adv. Funct. Mater.* 2020, **30**, 2003321.

[14] J. S. Jirkovsky´, I. Panas, E. Ahlberg, M. Halasa, S. Romani, D. J. Schiffrin; *J. Am. Chem. Soc.* 2011, **133**, 19432–19441.

[15] S. Siahrostami, A. Verdaguer-Casadevall, M. Karamad, D. Deiana, P. Malacrida, B. Wickman, M. Escudero-Escribano, E. A. Paoli, R. Frydendal, T. W. Hansen, I. Chorkendorff, I. E. L. Stephens, J. Rossmeisl; *Nat. Mater.* 2013, **12**, 1137–1143.

[16] Q. Chang, P. Zhang, A. H. Bagherzadeh Mostaghimi, X. Zhao, S. R. Denny, J. H. Lee, H. Gao, Y. Zhang, H. L. Xin, S. Siahrostami, J. G. Chen, Z. Chen; *Nat. Commun.* 2020, **11**, 2178.

[17] X. Zhou, B. Shen, J. Zhai, J. C. Conesa; *Small Methods* 2021, **5**, 2100269.

[18] D. Deng, L. Yu, X. Chen, G. Wang, L. Jin, X. Pan, J. Deng, G. Sun, X. Bao; *Angew. Chem. Int. Ed.* 2013, **52**, 371-375.

[19] M. V. Bracamonte, M. Melchionna, A. Stopin, An. Giulani, C. Tavagnacco, Y. Garcia, P. Fornasiero , D. Bonifazi , M. Prato; *Chem. Eur. J.* 2015, **21**, 12769-12777.

[20] G. Wu, K. L. More, C. M. Johnstonand, P. Zelenay; *Science* 2011, **332**, 443-447.

[21] H. Jiang, Y. Liu, J. Hao, Y. Wang, W. Li, J. Li; *ACS Sustainable Chem. Eng.* 2017, **5**, 5341–5350.

[22] M. Melchionna, P. Fornasiero, M. Prato; *Adv. Mater*. 2019, **31**, 180292.

[23] Y. Liu, X. Quan, X. Fan, H. Wang, S. Chen; *Angew. Chem. Int. Ed.* 2015, **5**, 6837–6841.

[24] M. Qiao, C. Tang, G. He, K. Qiu, R. Binions, I.P. Parkin, Q. Zhang, Z. Guo, M. M. Titirici; *J. Mater. Chem. A* 2016, **4**, 12658–12666.

[25] K. Gong, F. Du, Z. Xia, M. Durstock, L. Dai; *Science* 2009, **323**, 760–764.

[26] X. Liu, L. Dai; *Nat. Rev. Mater.* 2016, **1**, 16064.

[27] L. Dai, Y. Xue, L. Qu, H.-J Choi, J.-B Baek; *Chem. Rev.* 2015, **115**, 4823–4892.

[28] L. Qu, Y. Liu, J.-B Baek, L. Dai; *ACS Nano* 2010, **4**, 1321–1326.

[29] S. Iijima, Y. Yudasaka, R. Yamada, S. Bandow, K. Suenaga, F. Kokai, K. Takahashi; *Chem. Phys. Lett.* 1999, **309**, 165–170.

[30] W. Ding, Z. Wei, S. Chen, X. Qi, T. Yang, J. Hu, D. Wang, L.-J Wan, S.F. Alvi, L. Li; *Angew. Chem. Int. Ed.* 2013, **52**, 11755–11759.

[31] S. Yang, X. Feng, X. Wang, K. Müllen; Angew. Chem. Int. Ed. 2011, 50, 5339–5343.

[32] A. Dorjgotov, J. Ok, Y. Jeon, S.-H Yoon, Y. G. Shul; *J. Appl. Electrochem.* 2013, **43**,

387–397.

[33] A. Dumitru, M. Mamlouk, K. Scott; *Electrochim. Acta* 2013,

135, 428–438.

[34] W. Cai, Y. Wang, C. Xiao, H. Wu, X. YU; *Plasma Sci. Technol.* 2021, **23**, 025502.

[35] Y. Liu, J. Zhang, S. He, Y. Cui, L. Guan; *J. Energy Chem.*, 2021, **54**, 118–123.

[36] K. Dong, Y. Lei, H. Zhao, J. Liang, P. Ding, Q. Liu, Z. Xu, S. Lu, Q. Li, X. Sun; *J. Mater. Chem. A*, 2020, **8**, 23123.

[37] K. Sun, W. Xu, X. Lin, S. Tian, W.-F. Lin, D. Zhou, X. Sun; Adv. Mater. Interfaces 2021, 8, 2001360.

[38] J. Zhang, G. Zhang, S. Jin, Y. Zhou, Q. Ji, H. Lan, H. Liu, J. Qu; *Carbon* 2020, **163**, 154-161.

[39] M. Ferrara, M. Bevilacqua, M. Melchionna, A. Criado, M. Croser, C. Tavagnacco, F. Vizza, P. Fornasiero; *Electrochim. Acta* 2020, **364**, 137287.

[40] Y. Wang, R. Shi, L. Shang, G. I. N. Waterhouse, J. Zhao, Q. Zhang, L. Gu, T. Zhang; *Angew. Chem. Int. Ed.* 2020, **59** , 13057-13062.

[41] Y. Wang, R. Shi, L. Shang, L. Peng, D. Chu, Z. Han. G. I. N. Waterhouse, R. Zhang, T. Zhang ; *Nano Energy*, 2022, **96**, 107046.

[42] J. Zhang, H. Yang, J. Gao, S. Xi, W. Cai, J. Zhang, P. Cui, B. Liu; *Carbon Energy* 2020, **2**, 276-282.

[43] N. Wang, S. Ma, P. Zuo, J. Duan, B. Hou; *Adv. Sci.* 2021, **8**, 2100076.

[44] A. Lenarda, M. Bevilacqua, C. Tavagnacco, L. Nasi, A. Criado, F. Vizza, M. Melchionna, M. Prato, P. Fornasiero; *ChemSusChem* 2019, **12**, 1664–1672.

[45] J. Zhang, H. Zhang, M.-J. Cheng, Q. Lu; *Small* 2020, **16**, 1902845.

[46] Y. Pang, H. Xie, Y. Sun, M.-M. Titirici, G.-L. Chai; *J. Mater. Chem. A*, 2020, **8**, 24996–25016.

[47] Q. Zhang, M. Zhou, G. Ren, Y. Li, Y. Li, X. Du; *Nat. Commun*. 2020, **11**, 1731.

[48] X. Zhang, Y. Xia, C. Xia, H. Wang; *Trends in Chemistry*, 2020, **2**, 10.

[49] C. Xia, Y. Xia, P. Zhu, L. Fan, H. Wang; *Science* 2019, **366**, 226–231.

[50] D. Iglesias, A. Giuliani, M. Melchionna, S. Marchesan, A. Criado, L. Nasi, M. Bevilacqua, C. Tavagnacco, F. Vizza, M. Prato, P. Fornasiero; *Chem* 2018, **4**, 18-19.

[51] Y. Sun, L. Silvioli, N. R. Sahraie, W. Ju, J. Li, A. Zitolo, S. Li, A. Bagger, L. Arnarson, X. Wang, T. Moeller, D. Bernsmeier, J. Rossmeisl, F. Jaouen, P. Strasser, *J. Am. Chem. Soc.* 2019, **141**, 12372- 12381.

- Electrochemistry allows the hydrogen peroxide production with e renewable energy
- Oxygen electroreduction reaction allows the on-site production hydrogen peroxide
- Up to 1% hydrogen peroxide can be obtained using only electricity, water and oxygen
- H_2O_2 electrosynthesis outperforms the antraquinone process in energy efficiency

Declaration of interests

☒ The authors declare that they have no known competing financial interests or personal relationships that could have appeared to influence the work reported in this paper.

☐ The authors declare the following financial interests/personal relationships which may be considered as potential competing interests: